Biochemical and Biophysical Research Communications 501 (2018) 703–710

Contents lists available at ScienceDirect

Biochemical and Biophysical Research Communications

journal homepage: www.elsevier.com/locate/ybbrc

Structure-based protein engineering of bacterial β-xylosidase to increase the production yield of xylobiose from xylose

Seokho Hong [a, 1], Myungok Kyung [b, c, 1], Inseong Jo [a], Yong-Ro Kim [b], Nam-Chul Ha [a, *]

[a] Research Institute for Agriculture and Life Sciences, Center for Food and Bioconvergence, Center for Food Safety and Toxicology, Department of Agricultural Biotechnology, Seoul National University, Seoul, 08826, Republic of Korea
[b] Center for Food and Bioconvergence, Department of Biosystems & Biomaterials Science and Engineering, College of Agriculture and Life Sciences (CALS), Seoul National University, Seoul, 08826, Republic of Korea
[c] R&D Center, TS Corporation, 116, Incheon, 22300, Republic of Korea

ARTICLE INFO

Article history:
Received 30 April 2018
Accepted 9 May 2018

Keywords:
β-Xylosidase
Bacillus pumilus
Crystal structure
Xylobiose
Protein engineering
Disaccharide production

ABSTRACT

Xylobiose consists of two molecules of xylose and has been highly recognized as a food supplement because it possesses high prebiotic functions. β-xylosidase exhibits enzymatic activity to hydrolyze xylobiose, and the enzyme can also catalyze the reverse reaction in the presence of high concentrations of xylose. Previously, β-xylosidase from *Bacillus pumilus* IPO (BpXynB), belonging to GH family 43, was employed to produce xylobiose from xylose. To improve the enzymatic efficiency, this study determined the high-resolution structure of BpXynB in a complex with xylobiose and engineered BpXynB based on the structures. The structure of BpXynB deciphered the residues involved in the recognition of the xylobiose. A site-directed mutation at the residue for xylobiose recognition increased the yield of xylobiose by 20% compared to a similar activity of the wild type enzyme. The complex structure of the mutant enzyme and xylobiose provided the structural basis for a higher yield of the engineered protein. This engineered enzyme would enable a higher economic production of xylobiose, and a similar engineering strategy could be applied within the same family of enzymes.

1. Introduction

Plant cell walls are a complex mixture consisting mainly of cellulose, hemicellulose, and lignin [1]. Xylan is the major non-cellulosic polysaccharide of hemicellulose and constitutes ~30% of the total cell wall dry mass [2]. The backbone of xylan is made of a linear polymer of xyloses linked by β-1,4-glycosidic bonds, and its degradation requires a series of enzymatic actions. β-1,4-xylosidases belonging to the GH43 family have been found in diverse bacteria. These enzymes catalyze the release of xylose units from the non-reducing end of short xylooligosaccharides. The crystal structure of β-1,4-xylosidase from the thermophilic bacteria *Geobacillus stearothermophilus* T-6 (GsXynB3) was determined [3]. The structure revealed that each protomer consists of two domains with a tight dimeric assembly.

Xylooligosaccharides are low-calorie and are used as a soluble dietary fiber because they cannot be broken down by enzymes in the human digestive system [1,4]. Xylobiose (X2) has been utilized as a higher value food supplement, as it has the highest prebiotic ability among xylooligosacharides and is better than that of other non-digestible oligosaccharides for the proliferation of *Bifidobacteria* in the human gut [4–7]. While β-1,4-xylosidases can hydrolyze X2, the enzyme can also catalyze the production of an X2 molecule from two xylose molecules in the presence of high concentrations of xylose. In the latest study, the X2 reaction yield using β-1,4-xylosidase from *Bacillus pumilus* IPO (BpXynB) was 17% in a solution containing 90% (w/v) xylose [8].

To enhance the X2 production yield with BpXynB, we employed a structure-based protein engineering approach. We determined the crystal structures of BpXynB at high resolutions, elucidating the substrate-binding pocket and substrate interacting residues. Based on this structural information, BpXynB was engineered to make

* Corresponding author.
E-mail address: hanc210@snu.ac.kr (N.-C. Ha).
[1] Both authors contributed equally to this work.

https://doi.org/10.1016/j.bbrc.2018.05.051
0006-291X/

more interactions with the second xylose unit at the entrance of the substrate-binding pocket.

2. Materials and methods

2.1. Protein expression and purification

We used the plasmid for expression of the wild type BpXynB inserted in a pET21a vector (Novagen, USA), which was described previously [8]. The procedure of protein expression and purification was included in the Supplementary materials.

2.2. Site-directed mutagenesis

To construct the expression vector for the mutant BpXynB proteins (E186Q, F503Y, and E186Q/F503Y), site-directed mutagenesis was performed with *n*Pfu-Special polymerase chain reaction (PCR) premix (Enzynomics, Republic of Korea) and Dpn1 restriction enzyme using the plasmid for the wild type or E186Q mutant enzyme.

2.3. Crystallization and data collection

Single crystals of BpXynB were obtained by the hanging-drop vapor diffusion method using a precipitant solution containing 0.05 M HEPES (pH 8.0), 15% (w/v) polyethylene glycol (PEG) 3350, and 1% (w/v) tryptone. Equal volumes (1 μl) of the protein solution (7 mg/ml) and the reservoir solution were mixed and equilibrated against 500 μl reservoir solution at 14 °C. Single crystals of BpXynB-E186Q (12 mg/ml) and BpXynB-E186Q/F503Y (10 mg/ml) were obtained with a precipitant consisting of 0.05 M HEPES (pH 7.5), 20% (w/v) PEG 3350, 1% (w/v) tryptone, and 30 mM X2, which was obtained from TS Corporation Co., LTD (Incheon, Republic of Korea). Crystals of BpXynB, BpXynB-E186Q/X2, and BpXynB-E186Q/F503Y/X2 appeared after 1 day and were cryoprotected in precipitant solutions supplemented with 25% (v/v) glycerol, 25% (v/v) 2-methyl-2,4-pentanediol (MPD), and 30% (v/v) MPD, respectively, and flash-cooled in a liquid nitrogen stream at −173 °C. X-ray diffraction data sets were collected on beamline 5C and 7A at Pohang Accelerator Laboratory (PAL) (Pohang, Republic of Korea).

2.4. Structural determination and refinement

X-ray diffraction data were processed using HKL2000 software [9]. The structure of BpXynB was determined by the molecular replacement method with MOLREP in the CCP4 package [10] using the structure of β-1,4-xylosidase from *Bacillus subtilis* (PDB code: 1YIF; New York SGX Research Center for Structural Genomics, unpublished data) as a search model. The final structure of BpXynB was refined with PHENIX software suite [11]. The structures of BpXynB-E186Q and BpXynB-E186Q/F503Y were determined by the molecular replacement method using the wild type structure of BpXynB as a search model. X-ray diffraction and refinement statistics are presented in Table 1.

2.5. Multi-angle light scattering analysis

High-performance liquid chromatography (TSK-gel-G3000SWXL column, Tosoh Corporation, Japan) equipped with a multi-angle light scattering (MALS) instrument (Wyatt DAWN Heleos II (18 angles), USA) was employed. The protein sample (4 mg/ml) was applied to the column in a buffer containing 20 mM HEPES (pH 7.0), and 150 mM NaCl. Data analyses were performed with ASTRA 6 software (WYATT, USA).

2.6. Enzyme kinetic assays

The protein 5 μM in 100 mM sodium phosphate buffer (pH 6.5) was prepared as the enzyme solution, and 4-nitrophenyl β-D-xylopyranoside (pNPX) (Tokyo Chemical Industry, Japan) in DDW was prepared as the substrate solutions (0.05 mM, 0.5 mM, 1 mM, and 1.5 mM). Enzyme reactions were initiated by the addition of 50 μl of the substrate solution into 150 μl of the enzyme solution at room temperature. The amount of the chromogenic reaction

Table 1
X-ray diffraction and refinement statistics.

	wild type BpXynB	BpXynB-E186Q	BpXynB-E186Q/F503Y
Data collection			
Beam line	PAL 5C	PAL 7A	PAL 5C
Wavelength (Å)	0.99990	0.97934	0.97940
Space group	*C*2	*P*2	*C*2
Cell dimensions			
a, *b*, *c* (Å)	115.3, 105.2, 105.8	103.6, 105.2, 113.9	116.1, 103.1, 104.0
β(°)	122.7	111.0	122.7
Resolution (Å)	20.0–1.73 (1.76–1.73)	20.0–2.00 (2.03–2.00)	20.0–1.78 (1.81–1.78)
Rmerge	0.080 (0.294)	0.071 (0.334)	0.085 (0.466)
$I/\sigma I$	17.23 (2.63)	16.64 (2.84)	13.86 (1.97)
Completeness (%)	97.5 (92.1)	94.6 (88.7)	96.1 (88.8)
Redundancy	4.7 (3.0)	4.4 (2.8)	4.7 (2.6)
Refinement			
Resolution (Å)	47.2–1.73	30.7–2.00	35.6–1.78
No. reflections	98865	136082	83428
R_{work}/R_{free}	0.155/0.188	0.168/0.214	0.166/0.210
No. of Total atoms	9627	18426	9219
Wilson B-factor (Å)	16.9	22.2	16.7
R.M.S deviations			
Bond lengths (Å)	0.007	0.004	0.007
Bond angles (°)	0.875	0.713	0.916
Ramachandran plot			
Favored (%)	95.2	94.5	95.2
Allowed (%)	4.6	5.0	4.5
Outliers (%)	0.2	0.5	0.3
PDB ID	5ZQJ	5ZQX	5ZQS

product, *p*-nitrophenol, was estimated by measuring absorbance with GeneQuant 1300 spectrophotometer (GE Healthcare, USA) [12]. The absorption coefficient value of *p*-nitrophenol is 0.2 $mM^{-1}cm^{-1}$ at 405 nm, and values of V_{max} and K_m were determined by Lineweaver-Burk plot with linear regression analysis.

2.7. X2 production from xylose using BpXynB

To produce X2 from xylose using BpXynB, we applied a similar procedure as previously performed [8]. The specific procedure of X2 production was included in the Supplementary materials.

3. Results

3.1. Crystal structure of wild type BpXynB

We determined the crystal structure of wild type BpXynB at 2.0 Å resolution in the space group of *C*2, with the unit-cell dimensions $a = 115.3$, $b = 105.2$, $c = 105.8$ Å and $\beta = 122.7°$ (Table 1). Two molecules of the proteins were contained in the asymmetry unit (Fig. 1A). The overall structure of the protomer is similar to those of the GH43 family proteins [3,13–20]. The protomer consists of the N-terminal five-bladed β-propeller domain (residues 1–318) and the C-terminal β-sandwich domain (residues 327–535), which are connected by a long loop (residues 319–326) (Fig. 1). The N-terminal domain is composed of five β-sheets that are radially oriented, forming a complete circle. The C-terminal domain is made up of two anti-parallel β-sheets, one of which is highly curved (Fig. 1B).

The two protomers in the asymmetric unit strongly interact. The N-terminal domain interacts with the C-terminal domain of the other protomer in the dimer (Fig. 1A). For the dimeric assembly, two loops in the top region of the blades II and III are partially inserted into the long groove of the C-terminal domain of the other subunit in the dimer (Fig. 1A). The putative substrate-binding pockets were in the top region, surrounded by the connecting loops of β-strands of the N-terminal domain. One loop (residues 493–507, marked by *asterisk* in Fig. 1C) of the C-terminal domain also participated in the substrate-binding pocket. Interestingly, three glycerol molecules were found in each protomer, one of which interacts with the residues (Asp14, Asp127, and Arg287) in the substrate-binding pocket (Fig. 1C). The glycerol molecules seem to have been incorporated from the cryo-protectant solution during the X-ray diffraction data collection.

3.2. X2-bound structure of BpXynB-E186Q

To identify the residues involved in the recognition of X2, we determined the crystal structure in complex with X2 using a catalytic mutant protein to keep X2 in the substrate-binding pocket

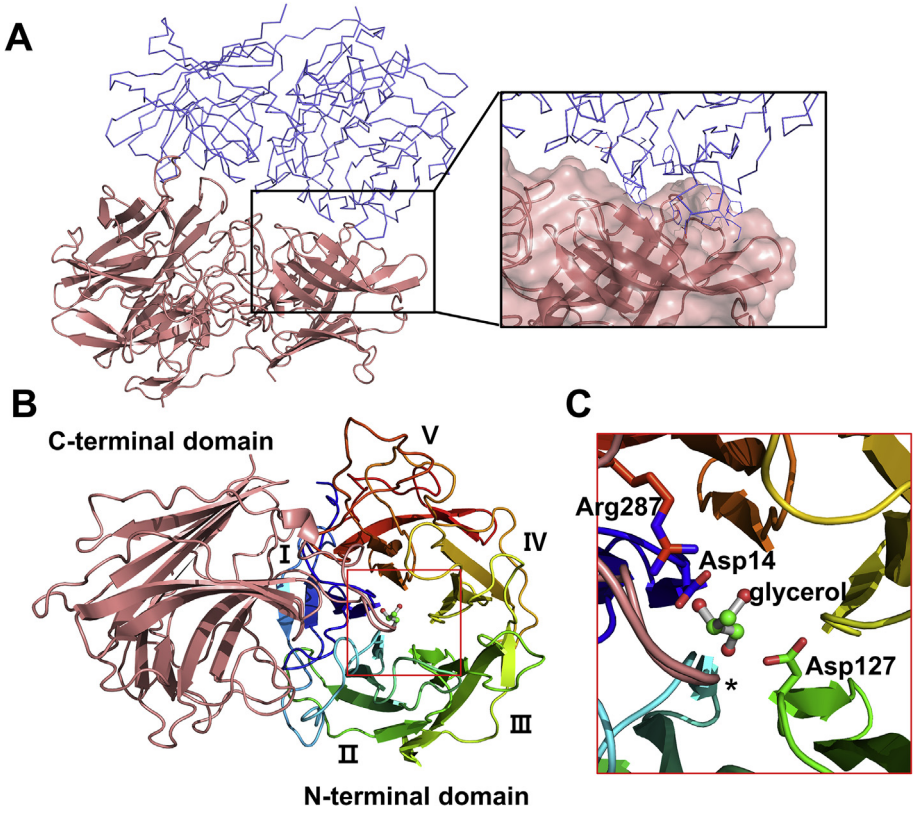

Fig. 1. Dimeric structure of BpXynB.
(A) The asymmetric unit of wild type BpXynB in the *C*2 space group. Two protomers are tightly bound (one protomer is in the ribbon representations (*pink*), and the other protomer is in the Cα representation (*blue*)). Glycerol molecules are shown as the stick model (*green*).
(B) Structure of the protomer consisting of the N-terminal β-propeller domain (1–318, *blue* to *red*) and the C-terminal β-sandwich domain (327–535, *pink*). The blades of the β-propeller domain are numbered I to V.
(C) The putative substrate-binding pocket lined by the loops from the N- and C- terminal domains. One glycerol molecule (stick model) was bound in the pocket. Three catalytic residues (Asp14, Asp127, and Arg287) are shown with the interacting glycerol molecule. (For interpretation of the references to colour in this figure legend, the reader is referred to the Web version of this article.)

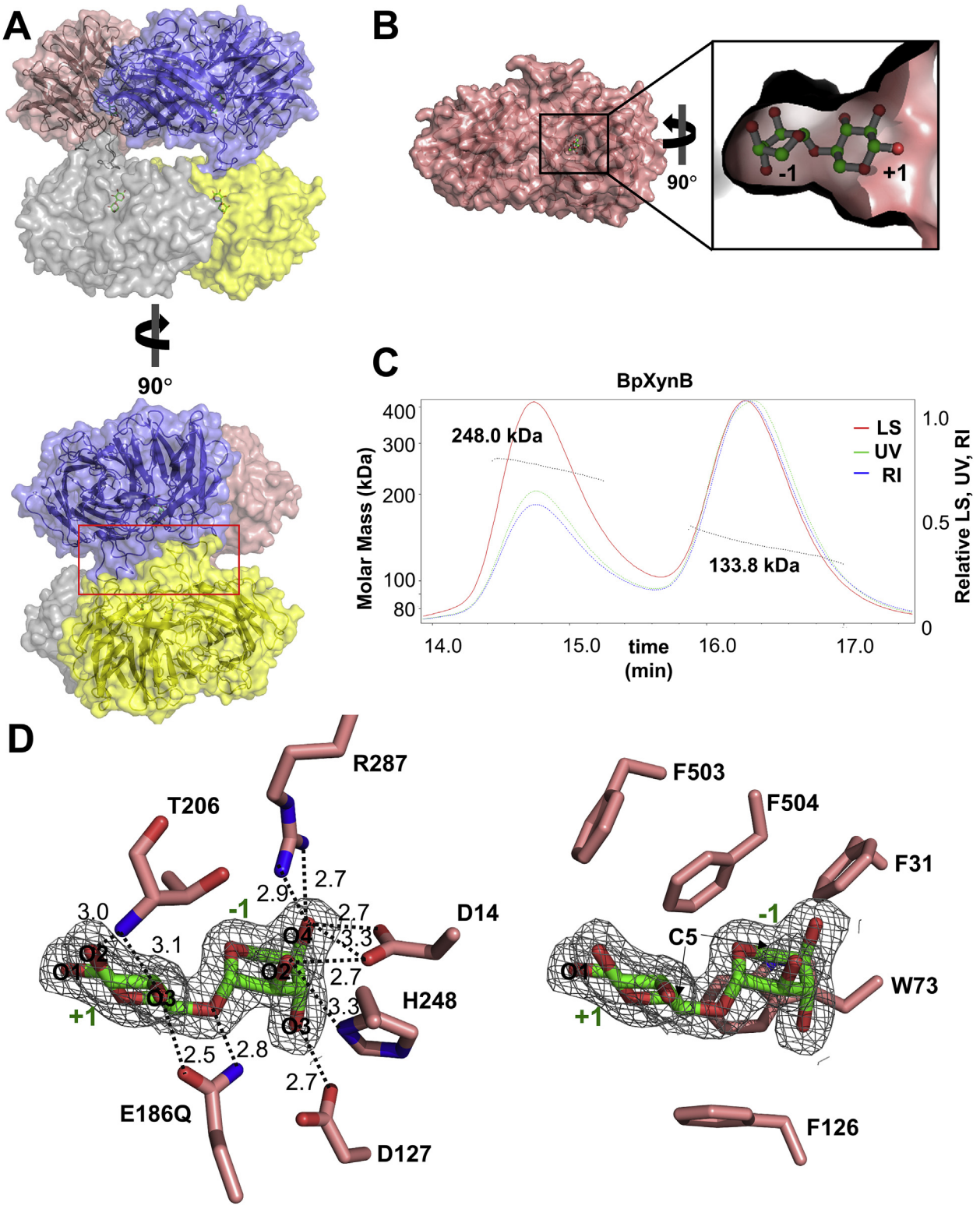

Fig. 2. The oligomeric states and X2 binding environment of BpXynB-E186Q.

(A) The asymmetric unit structure of BpXynB-E186Q in complex with X2. The four substrate-binding pockets are in the central cavity of the tetramer. Each protomer is represented as a transparent surface and/or ribbon model (*pink*, *blue*, *gray*, and *yellow*, respectively). Two protomers (*pink* and *blue*) form a dimer, and the other protomers (*gray* and *yellow*) form another dimer. X2's are represented as the stick model (*green*).

(B) The substrate-binding pocket of BpXynB-E186Q was shown in the surface representation (*pink*). The inset shows X2 (stick model), which was located in the substrate-binding pocket.

(C) The molecular sizes of the protein in the peaks were measured by using SEC-MALS. The peaks correspond to the molecular sizes of 248.0 kDa (~tetramer) and 133.8 kDa (~dimer), respectively.

(D) The hydrogen bonds (*left*) and the hydrophobic interactions (*right*) with X2 in the substrate-binding pocket. The residues (*pink*) involved in the interactions and X2 (*green*) are shown as stick model. Electron density maps of X2 are shown as a gray mesh and contoured at 1.0 σ. (For interpretation of the references to colour in this figure legend, the reader is referred to the Web version of this article.)

during the crystallization. Glu186, which was expected to be the nucleophilic catalytic residue based on the sequence comparison, was changed to glutamine. As expected, the E186Q mutation abolished X2 hydrolyzing activity of the protein. The crystals of the X2-bound form of BpXynB-E186Q were obtained by adding 30 mM X2 in the reservoir solution, and the complex structure was determined at 2.0 Å resolution with the crystals that have a different space group from the wild type structure. Four molecules were contained in the asymmetric unit, which exhibited close contact between two dimers via loops making a central hollow (Fig. 2A).

The overall structure of the BpXynB-E186Q/X2 protomer was very similar to that of the wild type enzyme (rmsd = 0.129 Å between 471 Cα residues). X2 was tightly bound in the substrate-binding pocket by both hydrogen bonds and hydrophobic interactions (Fig. 2B and D). The side chains of Asp14, Asp127, Glu186 (Gln186 in the mutant enzyme), His248, and Arg287 participated in binding to X2 with the backbone amide group of Thr206 (Fig. 2D, *left*). Of these, Asp14, Asp128, and Glu186 were characterized as catalytically important residues in GsXynB3 [3]. Phe31, Trp73, and Phe126 from the N-terminal domain, and Phe503 and Phe504 from the C-terminal domains made the hydrophobic contacts with X2 (Fig. 2D, *right*).

The substrate-binding pocket can be divided into two subsites: −1 subsite for the non-reducing sugar (or glycon xylose unit) and +1 subsite for the reducing sugar (or aglycon xylose unit) (Fig. 2D). The glycon xylose unit at the −1 subsite adopts a $^{1}C_{4}$ chair conformation (C1 is above the plane of the chair and C4 carbon is below the plane). The aglycon xylose unit at +1 subsite adopts a different isomeric chair conformation, a $^{4}C_{1}$ chair conformation (C4 is above and C1 is below the plane of the chair). At the front face of the −1 subsite, the 2-O and 4-O of the glycon xylose are fixed by an extensive hydrogen bonding network consisting of Asp14, His248, and Arg287. At the back face of the −1 subsite, the 3-O of the glycon xylose forms a hydrogen bond with Asp127. The oxygen at the glycosidic bond and the 3-O of the xylose unit at the reducing end make the hydrogen bond with the nucleophilic catalytic residue, Glu186, at the +1 subsite. The 3-O also interacts with the backbone amide group of Thr206, which forms a hydrogen bond with the 2-O of the aglycon xylose unit (Fig. 2D, *left*). The hydrophobic CH_2 moieties at the C5 carbon of both xylose units are stabilized by the side chains of Trp73 and Phe504 residues. Phe503 forms

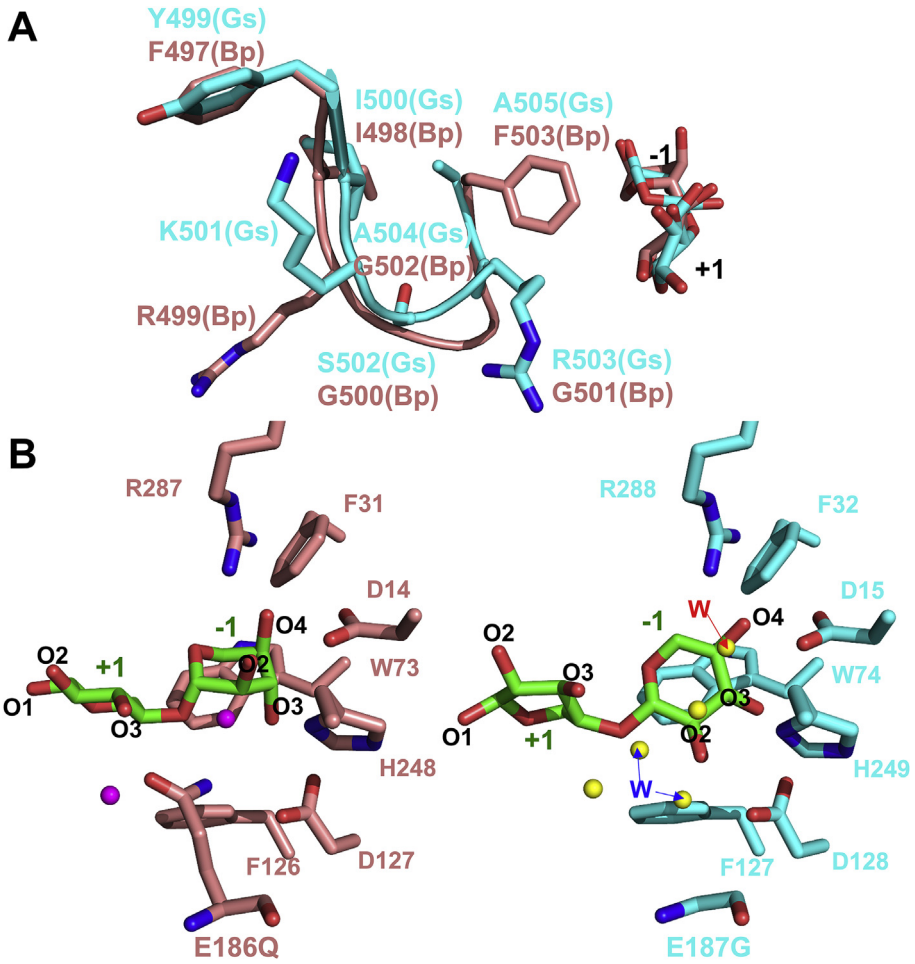

Fig. 3. Comparison of the substrate-binding pockets between BpXynB and GsXynB3.
(A) The loop from the C-terminal β-sandwich domain of BpXynB (residues 497–503; FIRGGGF, *pink*) has a different sequence and conformation compared to that of GsXynB3 (residues 499–505; YIKSRAA, *cyan*). The three-dimensional model of GsXynB3 was retrieved from Protein Data Bank (PDB code 2EXK; the crystal structure of GsXynB3-E187G/xylobiose [3]), and the crystal structure of BpXynB-E186Q in complex with X2 was used. The X2 molecules in the substrate-binding pockets are shown as the stick model.
(B) The glycon xylose unit of BpXynB (*left*, *pink*) adopts the alternative chair conformation with all hydroxyl groups in the axial conformation; however, the xylose unit at the −1 subsite of GsXynB3 (*right*, *cyan*) adopts the chair conformation with all hydroxyl groups in the equatorial orientation. Water molecules are shown in the spheres (*magenta* from BpXynB, *yellow* from GsXynB3) and X2 molecules are shown in the stick (*green*). (For interpretation of the references to colour in this figure legend, the reader is referred to the Web version of this article.)

hydrophobic interactions with Phe504 and points to the C-1 hydroxyl group of the reducing end xylose unit (Fig. 2D, *right*).

3.3. Oligomeric state determination of BpXynB

As mentioned above, the asymmetric unit of the crystal structure of BpXynB-E186Q/X2 contained a tetramer consisting of two dimeric units (Fig. 2A). The tetrameric structure was stabilized by the interactions between the loops coming from the top region of the blades IV and V of the N-terminal domain of one protomer (*blue*) and the loops from a protomer (*yellow*) of the other dimer. Interestingly, the tetramer has a large cavity in its center with large holes on both side and all four active sites are in the central cavity (Fig. 2A). Therefore, only short chains of xylooligosaccharides can access to the active sites.

To investigate the oligomeric states of BpXynB in a solution, the wild type of the BpXynB protein was subjected to multi-angle light scattering (MALS) analysis. Both tetrameric (248.0 kDa, 32% (w/w)) and dimeric (133.8 kDa, 68% (w/w)) forms co-existed in solution (Fig. 2C). The tetrameric structure appears to be advantageous in the cooperative digestion of the substrate due to the multiple active sites in the cavity. However, long or bundled xylooligosaccharides would not enter to the central cavity, because they could not pass through the holes into the central cavity. In contrast, the dimeric form of BpXynB could be more efficient in hydrolyzing the larger substrates but with less cooperation. Thus, co-existence of the tetrameric and dimeric BpXynB would help digestion of diverse forms of xylooligosaccharides.

3.4. Structural comparison to GsXynB3

Structural superposition with the GsXynB3 structure (sequence identity 65%) [3] revealed that a loop (residues 497–503 in the BpXynB and residues 499–505 in the GsXynB3) at the substrate-binding pocket from C-terminal domain is significantly different each other (Fig. 3A). The glycine residues (Gly500-Gly501-Gly502) in the loop of BpXynB were rendered more flexible than that of GsXynB3, which has Ser502-Arg503-Ala504 residues instead. The bulkier Phe503 in the BpXynB loop occupies more space within the substrate-binding pocket than the Ala505 residue in the GsXynB3 loop.

Apparent conformational difference was also found in the bound X2s. Both xylose units at the −1 subsite and the +1 subsite in GsXynB3 adopted a chair conformation with all hydroxyl groups in the equatorial orientation. However, the glycon xylose unit at the −1 subsite of BpXynB adopted the alternative chair conformation with the C-2, C-3, and C-4 hydroxyl groups in the axial conformation, and the all hydroxyl groups of the aglycon xylose unit at the +1 subsite were in the equatorial orientation similar to the xylose unit in GsXynB3 (Fig. 3B). These alternative chair conformations of the xylose unit at the −1 subsite may result from the different mutation of amino acids. The catalytic Glu186 residue of BpXynB was mutated as Gln186 in this study. However, the corresponding residue of GsXynB3 (Glu187) was mutated as glycine, which is smaller and occupies less space than glutamate. As a result, the xylose unit at the −1 subsite of GsXynB3 can change the orientation of hydroxyl groups from axial to equatorial, and there were an additional three water molecules found. Two water molecules (W in *blue*) occupied the space of the Glu187 side chain, and one water molecule (W in *red*) was located in the position of the 2-O of the glycon xylose unit at the −1 subsite of BpXynB (Fig. 3B).

3.5. BpXynB F503Y variant exhibits higher efficiency in production of X2 from xylose

We hypothesized that tighter binding of xylose at the +1 subsite contributes to efficient production of X2 by facilitating the combination of two xylose molecules at the substrate-binding pocket. In this study, we noted the Phe503 residue in the +1 subsite (Fig. 4, *orange*). Since the phenyl ring of Phe503 points to the 1-O of xylose at the +1 subsite without any polar interaction, we expected that the mutation to tyrosine would result in better interaction with the aglycon xylose unit through the interaction between the hydroxyl group of tyrosine and the 1-O of xylose at the +1 subsite.

The F503Y variant enzyme (BpXynB-F503Y) was overproduced and compared to the catalytic activity of the wild type enzyme. The V_{max} value of the mutation decreased by approximately 9% when pNPX was used as a substrate, compared to the wild type enzyme. However, the K_m value of BpXynB-F503Y was increased 2.2-fold when compared with the wild type enzyme (Table 2). The higher K_m value may be associated with a lower affinity for the pNPX or X2, and X2 that is synthesized by BpXynB-F503Y may be less hydrolyzed by the mutant enzyme. To measure the X2 production yield from xylose, the enzymes were treated in 90% xylose solution for

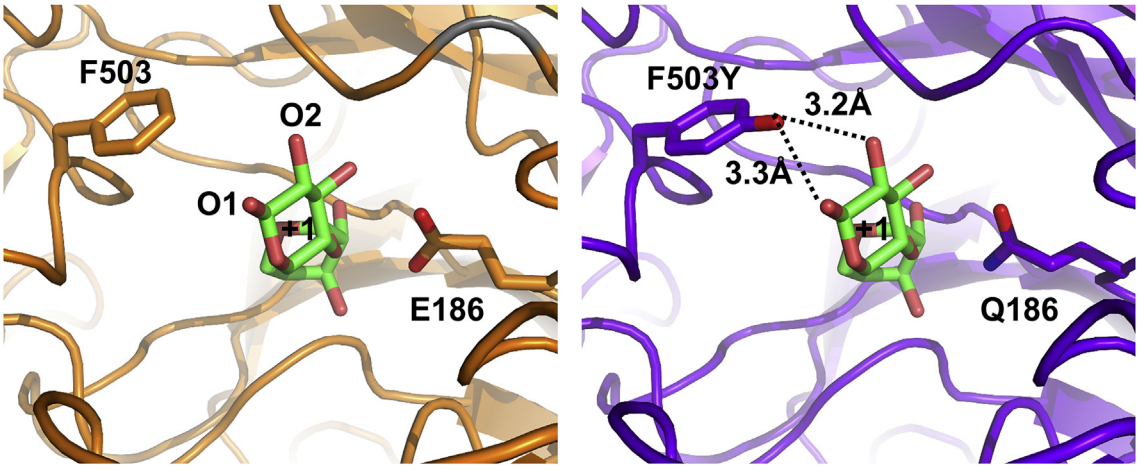

Fig. 4. The X2 recognition in BpXynB-F503Y.
(A) Phe503 of the wild type of BpXynB (*left, orange*) and F503Y of BpXynB-E186Q/F503Y (*right, purple*). F503Y makes additional hydrogen bonds with 1-O and 2-O of the aglycon xylose at the +1 subsite of substrate-binding pocket. X2 molecules (*green*) were retrieved from the crystal structure of BpXynB-E186Q/F503Y/X2. (For interpretation of the references to colour in this figure legend, the reader is referred to the Web version of this article.)

Table 2
Enzyme kinetic assays and X2 reaction yield.

Enzyme	kinetic parameters			X2 yield (%)
	Regression Line	V_{max} (mM/min)	K_m (mM)	
BpXynB wild type	$y = 0.0586x + 0.0393$ $R^2 = 0.9996$	25.4	1.49	13.5
BpXynB F503Y	$y = 0.1402x + 0.0433$ $R^2 = 0.9996$	23.1	3.24	16.4

y: 1/reaction velocity (mM/min), x: 1/substrate concentration (mM).

24 h at 1 U/ml. The mutant enzyme converted 16.4% of xylose into X2, which is a higher conversion yield than the wild type enzyme by 21% (Table 2).

3.6. Structural basis for the tighter binding of the xylose unit at the +1 subsite of the F503Y mutant

To evaluate the structural basis for the higher production yield of F503Y mutant enzyme, we determined the crystal structure of BpXynB-E186Q/F503Y/X2. To obtain the co-crystallized complex structure of BpXynB-F503Y, Glu186 was mutated to Gln186 in order to construct the non-catalytic mutant, BpXynB-E186Q/F503Y. Overall shapes of BpXynB and BpXynB-E186Q/F503Y/X2 are approximately the same (rmsd = 0.135 Å between 498 Cα residues), and the oligomeric structure of BpXynB-E186Q/F503Y/X2 was also a dimer, similar to BpXynB. As intended, additional hydrogen bonding interactions were observed between Phe503, and 1-O and 2-O of the aglycon xylose at the +1 subsite in the substrate-binding pocket (Fig. 4, *purple*).

4. Discussion

In this study, we determined the crystal structure of BpXynB, with and without X2, to analyze the X2 binding environment at the atomic level. The deep substrate-binding pocket was surrounded by the connecting loops from the N-terminal domain and one loop from the C-terminal domain. Structural and sequence comparison to GsXynB3 revealed a substantial difference in the loop from the C-terminal domain. The Phe503 in the loop was replaced with Ala505 in GsXynB3, which made a broader substrate-binding pocket in GsXynB3. At the −1 subsite of the substrate-binding pocket, there are extensive hydrogen bond networks between hydrophilic residues and the glycon xylose unit. However, less extensive interactions were found at the +1 subsite. To combine two xylose molecules for the production of X2, two xylose molecules should be bound in the substrate-binding pocket at once. We noted Phe503 at the entrance of the X2 binding pocket in order to create a better fit for the loosely bound xylose unit at the +1 subsite. We attempted to add hydrogen bonds at the Phe503 site by changing the residue to tyrosine. Indeed, the F503Y mutant enzyme improved the production yield of X2 from xylose, which was confirmed by the crystal structure of the mutant in complex with X2 at the atomic level. Our finding demonstrates that the tighter binding of the second, or aglycon, sugar is important in promoting the reverse reaction of hydrolase. Thus, the mutation at the +1 subsite, which was introduced in this study, could also be applied to protein engineering of the same GH43 family proteins, and other oligosaccharide hydrolases.

Currently, harsh and highly concentrated acids are widely used for the extraction and breakdown of xylan to produce xylooligosaccharides (XOS) [21]. An alternative approach was developed by combining two xylose molecules, which improved the process by applying simulated moving bed technology [8]. This alternative method was environmentally friendly and yielded higher purity than the conventional methods. If the F503Y mutant protein were used in this method, the amount of the enzyme would be reduced by 20% resulting in a more economic production of X2 from xylose. Moreover, the alternative method would be more beneficial to consumers because high purity X2 is more effective in prebiotic function than XOS. Thus, this approach has the potential to become a major method of X2 production in the future.

Acknowledgement

This research was supported by National Research Foundation of Korea (NRF-2017H1A2A1042661-Global Ph.D. Fellowship Program to SH) and by Korea Institute of Planning and Evaluation for Technology in Food, Agriculture, Forestry (IPET; 710012-03-1-HD120; ARC program to NCH). We made use of beamlines 5C and 7A at Pohang Accelerator Laboratory (Pohang, Republic of Korea), and the MALS facility at the Korea Basic Science Institute (Ochang, Republic of Korea).

Transparency document

Transparency document related to this article can be found online at https://doi.org/10.1016/j.bbrc.2018.05.051.

Appendix A. Supplementary data

Supplementary data related to this article can be found at https://doi.org/10.1016/j.bbrc.2018.05.051.

References

[1] M.J. Vazquez, J.L. Alonso, H. Dominguez, J.C. Parajo, Xylooligosaccharides: manufacture and applications, Trends Food Sci. Technol. 11 (2000) 387–393.
[2] H.V. Scheller, P. Ulvskov, Hemicelluloses, Annu. Rev. Plant Biol. 61 (2010) 263–289.
[3] C. Brux, A. Ben-David, D. Shallom-Shezifi, M. Leon, K. Niefind, G. Shoham, Y. Shoham, D. Schomburg, The structure of an inverting GH43 beta-xylosidase from Geobacillus stearothermophilus with its substrate reveals the role of the three catalytic residues, J. Mol. Biol. 359 (2006) 97–109.
[4] M. Okazaki, H. Koda, R. Izumi, S. Fujikawa, N. Matsumoto, In vitro digestibility and in vivo utilization of xylobiose, J. Jpn. Soc. Nutr. Food Sci. 44 (1991) 41–44.
[5] J. Jaskari, P. Kontula, A. Siitonen, H. Jousimies-Somer, T. Mattila-Sandholm, K. Poutanen, Oat beta-glucan and xylan hydrolysates as selective substrates for Bifidobacterium and Lactobacillus strains, Appl. Microbiol. Biotechnol. 49 (1998) 175–181.
[6] M. Okazaki, S. Fujikawa, N. Matsumoto, Effect of xylooligosaccharide on the growth of bifidobacteria, Bifidobacteria Microflora 9 (1990) 77–86.
[7] C.E. Rycroft, M.R. Jones, G.R. Gibson, R.A. Rastall, A comparative in vitro evaluation of the fermentation properties of prebiotic oligosaccharides, J. Appl. Microbiol. 91 (2001) 878–887.
[8] C. Park, J. Choi, M. Kyung, S. Seo, S.-E. Jo, K. Lee, P. Kim, N.-H.L. Wang, S. Jung, S. Mun, Application of Bacillus pumilus β-xylosidase reaction and simulated moving bed purification to efficient production of high-purity xylobiose from xylose, J. Ind. Eng. Chem. 47 (2017) 431–438.
[9] Z. Otwinowski, W. Minor, Processing of X-ray diffraction data collected in oscillation mode, Methods Enzymol. 276 (1997) 307–326.
[10] M.D. Winn, C.C. Ballard, K.D. Cowtan, E.J. Dodson, P. Emsley, P.R. Evans, R.M. Keegan, E.B. Krissinel, A.G. Leslie, A. McCoy, S.J. McNicholas, G.N. Murshudov, N.S. Pannu, E.A. Potterton, H.R. Powell, R.J. Read, A. Vagin, K.S. Wilson, Overview of the CCP4 suite and current developments, Acta Crystallogr. Sect. D Biol. Crystallogr. 67 (2011) 235–242.
[11] P.D. Adams, P.V. Afonine, G. Bunkoczi, V.B. Chen, I.W. Davis, N. Echols, J.J. Headd, L.W. Hung, G.J. Kapral, R.W. Grosse-Kunstleve, A.J. McCoy, N.W. Moriarty, R. Oeffner, R.J. Read, D.C. Richardson, J.S. Richardson, T.C. Terwilliger, P.H. Zwart, PHENIX: a comprehensive Python-based system for macromolecular structure solution, Acta Crystallogr. Sect. D Biol. Crystallogr. 66 (2010) 213–221.
[12] D. Shallom, M. Leon, T. Bravman, A. Ben-David, G. Zaide, V. Belakhov, G. Shoham, D. Schomburg, T. Baasov, Y. Shoham, Biochemical characterization and identification of the catalytic residues of a family 43 beta-D-xylosidase from Geobacillus stearothermophilus T-6, Biochemistry 44 (2005) 387–397.
[13] D. Nurizzo, J.P. Turkenburg, S.J. Charnock, S.M. Roberts, E.J. Dodson, V.A. McKie, E.J. Taylor, H.J. Gilbert, G.J. Davies, Cellvibrio japonicus alpha-L-arabinanase 43A has a novel five-blade beta-propeller fold, Nat. Struct. Biol.

9 (2002) 665–668.
[14] M. Till, D. Goldstone, G. Card, G.T. Attwood, C.D. Moon, V.L. Arcus, Structural analysis of the GH43 enzyme Xsa43E from Butyrivibrio proteoclasticus, Acta Crystallogr. Struct. Biol. Commun. 70 (2014) 1193–1198.
[15] E. Vandermarliere, T.M. Bourgois, M.D. Winn, S. van Campenhout, G. Volckaert, J.A. Delcour, S.V. Strelkov, A. Rabijns, C.M. Courtin, Structural analysis of a glycoside hydrolase family 43 arabinoxylan arabinofuranohydrolase in complex with xylotetraose reveals a different binding mechanism compared with other members of the same family, Biochem. J. 418 (2009) 39–47.
[16] L.S. McKee, M.J. Pena, A. Rogowski, A. Jackson, R.J. Lewis, W.S. York, K.B. Krogh, A. Vikso-Nielsen, M. Skjot, H.J. Gilbert, J. Marles-Wright, Introducing endo-xylanase activity into an exo-acting arabinofuranosidase that targets side chains, Proc. Natl. Acad. Sci. U. S. A. 109 (2012) 6537–6542.
[17] J.S. Brunzelle, D.B. Jordan, D.R. McCaslin, A. Olczak, Z. Wawrzak, Structure of the two-subsite beta-d-xylosidase from Selenomonas ruminantium in complex with 1,3-bis[tris(hydroxymethyl)methylamino]propane, Arch. Biochem. Biophys. 474 (2008) 157–166.
[18] A. Cartmell, L.S. McKee, M.J. Pena, J. Larsbrink, H. Brumer, S. Kaneko, H. Ichinose, R.J. Lewis, A. Vikso-Nielsen, H.J. Gilbert, J. Marles-Wright, The structure and function of an arabinan-specific alpha-1,2-arabinofuranosidase identified from screening the activities of bacterial GH43 glycoside hydrolases, J. Biol. Chem. 286 (2011) 15483–15495.
[19] Z. Fujimoto, H. Ichinose, T. Maehara, M. Honda, M. Kitaoka, S. Kaneko, Crystal structure of an Exo-1,5-{alpha}-L-arabinofuranosidase from Streptomyces avermitilis provides insights into the mechanism of substrate discrimination between exo- and endo-type enzymes in glycoside hydrolase family 43, J. Biol. Chem. 285 (2010) 34134–34143.
[20] M.R. Proctor, E.J. Taylor, D. Nurizzo, J.P. Turkenburg, R.M. Lloyd, M. Vardakou, G.J. Davies, H.J. Gilbert, Tailored catalysts for plant cell-wall degradation: redesigning the exo/endo preference of Cellvibrio japonicus arabinanase 43A, Proc. Natl. Acad. Sci. U. S. A. 102 (2005) 2697–2702.
[21] Q. Yuan, H. Zhang, Z. Qian, X. Yang, Pilot-plant production of xylo-oligosaccharides from corncob by steaming, enzymatic hydrolysis and nanofiltration, J. Chem. Technol. Biotechnol. 79 (2004) 1073.